Mechanisms and Dynamics of Mineral Dissolution

A New Kinetic Monte Carlo Model

Martin, Pablo; Manzano, Hegoi; Dolado, Jorge S.

Important note
To cite this publication, please use the final published version (if applicable).
Please check the document version above.

Mechanisms and Dynamics of Mineral Dissolution: A New Kinetic Monte Carlo Model

Pablo Martin, Hegoi Manzano,* and Jorge S. Dolado*

Mineral dissolution is a fundamental process in geochemistry and materials science. It is controlled by the complex interplay of atomic level mechanisms like adatoms and terraces removal, pit opening, and spontaneous vacancy creation that can be gradually activated at different energies. Though the development of a comprehensive atomistic model is key to go deeper into the understanding of this phenomenon, existing models have failed to reproduce the abrupt dependence of the dissolution rate with the Gibbs free energy (ΔG). Herein, a new atomistic kinetic Monte Carlo (KMC) model is presented, which, invoking the microscopic reversibility of chemical reactions, captures the experimentally observed sigmoid dependence of the dissolution rate and provides new insights on the concomitant dissolution mechanisms. As a salient result, the model predicts the possible existence of unreported close-to-equilibrium dissolution modes where spontaneous vacancies creation and pit opening can occur before adatom and terrace removal.

1. Introduction

Mineral dissolution has high relevance in countless important geophysical phenomena like soil formation,[1,2] water and petrol reservoir stability,[3,4] or carbon sequestration,[5–8] among others. To describe these phenomena is crucial to completely understand dissolution process, yet it presents some unanswered

P. Martin
Building Technologies Division Tecnalia
Parque Tecnológico de Bizkaia
Astondo Bidea, Edificio 700, CP 48160 Derio, Bizkaia, Spain

Dr. H. Manzano
Department of Condensed Matter Physics
University of the Basque Country UPV/EHU
Barrio Sarriena s/n, 48940 Leioa, Bizkaia, Spain
E-mail: Hegoi.manzano@ehu.eus

Dr. J. S. Dolado
Materials Physics Center - Centro de Física de Materiales CSIC-UPV/EHU
Paseo Manuel de Lardizabal, 5, 20018 San Sebastian, Spain
E-mail: Jorge_dolado002@ehu.eus

Dr. J. S. Dolado
Donostia International Physics Center
Paseo Manuel Lardizabal 3, 20018 San Sebastián, Spain

Dr. J. S. Dolado
Faculty of Civil Engineering and Geosciences
Delft University of Technology
Stevinweg 1, 2628 CN, Delft, The Netherlands

The ORCID identification number(s) for the author(s) of this article can be found under https://doi.org/10.1002/adts.201900114

issues. The dissolution of a solid material is a complex process which is simultaneously affected by the solid surface topology (exposed surface, nature of the atomic bonds, presence of impurities, defects, etc.) and the nature of the surrounding solution. Indeed, the driving force of dissolution is controlled by the Gibbs free energy (ΔG), which is closely related to the ion activity in the solvent.[9–16] From experiments, a sigmoidal shape dependence between dissolution rate and ΔG is generally obtained (see **Figure 1**c).[10,12–15,17,18] Different regions in the sigmoidal function seem to be governed by different dissolution mechanisms depending on the mineral cohesive energy and ΔG. These mechanisms can be observed experimentally when vertical scanning interferometry and atomic force or scanning electron microscopy are used to follow the surface topography during dissolution.[9,10,15,19,20] In a typical curve like the one portrayed in Figure 1c, three mechanisms with different dissolution rates can be distinguished:

– Mechanism I. At low negative ΔG adatoms and terraces dissolve leading to a flat surface. The dissolution rate is very low due to the close position to equilibrium state.
– Mechanism II. As ΔG decreases, vacancies and dislocations of the system become dissolution cores leading to pit opening and step retreat.
– Mechanism III. As ΔG becomes even lower, any surface atom can become a dissolution core. However, this only occurs in minerals with low cohesive energy.

The three dissolution mechanisms are supposed to be additive and must coexist, that is, it is not possible to have mechanism II without mechanism I, or mechanism III without II and I, and they take place simultaneously. The value of ΔG where the onset of dissolution rate takes place due to mechanism II is called critical ΔG (ΔG_{crit}).

Computational methods have played an important role in the last thirty years to give basic atomic level explanation to dissolution. In 1986 Lasaga and Blum studied the etch pits formation due to dislocations using a Monte Carlo (MC) method.[21] This implied the beginning of the so called flickering-bond model development where the dissolution rate is defined by the elementary bond-forming bond-breaking reactions.[19,22] About 10 years later,[23] the generalized use of kinetic Monte Carlo (KMC) method involved a great progress due to its faster computing

ADVANCED
SCIENCE NEWS
www.advancedsciencenews.com

ADVANCED
THEORY AND
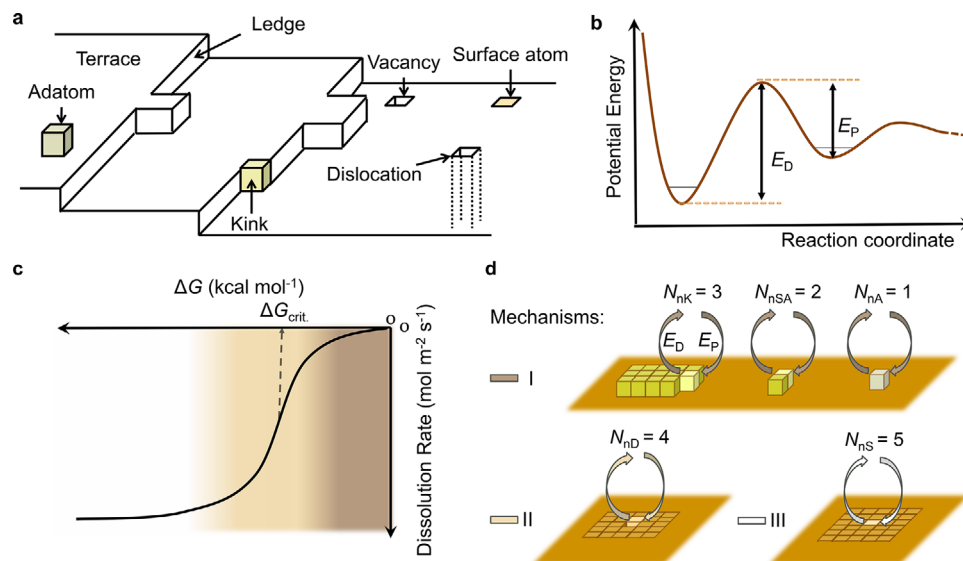**SIMULATIONS**
www.advtheorysimul.com

Figure 1. Schematic representation of mineral dissolution processes. a) Representation of a Kossel's surface with different topographic defects. Dotted lines represent an infinite hole. b) Potential energy curve in a typical dissolution process. Solid lines represent the fundamental frequency for the potential wells. c) Dissolution pathways versus ΔG of a mineral. The onset in dissolution rate due to mechanism II is given at ΔG_{crit}. d) The three generic dissolution mechanisms.[17] N_{nK} coordination number for a kink atom, N_{nSA} for a step adatom, N_{nA} for an adatom, N_{nD} for an atom close to a dislocation or step atom, and N_{nS} for a surface atom.

speed. For example, Liang et al. used KMC to consider explicitly the effects of structure and surface topography at the molecular scale in calcite,[24] and more recently, Kurganskaya and Luttge have used KMC to study silicate[25] and carbonate[26] minerals dissolution with atomistic detail at far from equilibrium conditions.

Common KMC models based on transition state theory (TST) consider that one atom, molecule or coarse-grained block is removed from the system.[11] The rate of this dissolution event, r_D, depends on its dissolution reaction energy barrier E_D.

$$r_D = \frac{k_B \cdot T}{\hbar} \cdot \exp\left(-\frac{E_D \cdot N_n}{k_B \cdot T}\right) \qquad (1)$$

where k_B is the Boltzmann constant, $\hbar$ the Planck constant, T the temperature, and N_n the number of first neighbors. $k_B \cdot T/\hbar$ is the commonly named fundamental frequency f_f. Despite their simplicity, TST-based KMC models allow to study minerals dissolution at far from equilibrium conditions. In fact, they capture the inherent topographies associated with the dissolution mechanisms,[25–28] permit the analysis of effects like dislocations,[27,28] grain sizes,[29] and particular mineral structures,[25,26] etc., and even reproduce the experimentally observed pulsating frequency at the nanoscale.[30]

It is generally accepted from the above mechanisms that the origin of the sigmoidal behavior with ΔG arises from the interplay between the mineral nanoscale topography and the ΔG itself. Previous works have regarded the study of dissolution rate dependence with ΔG by MC method by considering dissolution and precipitation separately,[22,31,32] failing to reproduce the dissolution mechanisms over the whole ΔG range. In this work an extension to the model has been proposed based on TST and microscopic reversibility (Equations (4) and (5)). The usual mineral–water reaction equation proposed by Lasaga[21,22] is

complemented, considering dissolution and precipitation events independently. For each event the rate depends on its specific energy barriers of dissolution or precipitation and the vicinity of the dissolved molecule.

For simplicity, the model has been applied to study the dissolution of a Kossel crystal. A Kossel crystal, or Terrace Ledge Kink system (TLK), is a simple mineral structure consisting of a cubic structure with six first neighbors[33] (see Figure 1a). Despite the simplicity of this system, it ensures enough topographical details so as to reproduce the mechanisms attributed to the dissolution process.

The paper is organized as follows: First, the net dissolution rate dependence with the main parameters of the model, that is, the dissolution and precipitation energy barriers, has been explored. As said before, the model is able to reproduce the sigmoid dissolution rate function with ΔG and the intrinsic mechanisms. Second, these microscopic parameters have been related to macroscopic parameters, like the dissolution onset ΔG_{crit}, or the effective activation energy E_a, readily accessible by experimental means. Finally, experimental data for several minerals have been fitted, finding a reasonable good agreement in spite of the structural limits of using a simple Kossel crystal.

1.1. Model Description

As is mentioned above, mineral dissolution depends on the equilibrium between the solid and the solution, represented by ΔG. At a microscopic level, the net dissolution rate is the result of the equilibrium between dissolution and precipitation. On the one hand, dissolution is related to mineral cohesive energy. On the other hand, precipitation varies with both mineral nature and

**ADVANCED
SCIENCE NEWS**
www.advancedsciencenews.com

**ADVANCED
THEORY AND
SIMULATIONS**
www.advtheorysimul.com

saturation grade of solvent. Dissolved atoms tends to stay close to the mineral, which leads to a high supersaturation state close to the surface, or what it is the same, to a low negative Gibbs free energy (ΔG) between mineral and solvent. Under these conditions, close to the surface there could be the possibility for an already dissolved atom or molecule to reform its bonds and come back to the material.[21] In equilibrium, dissolution and precipitation processes have the same probability, what is known as microscopic reversibility.[34] Bandstra and Brantley[35] used this idea to develop a simple 2D Ising model to study dissolution dependence with ΔG, achieving a good description. Following that idea, here it is suggested to divide the net dissolution into two processes described by the following equations:

$$r_D = f_f \cdot \exp\left(-\frac{E_D \cdot N_n}{k_B \cdot T}\right) \tag{2}$$

$$r_P = f_f \cdot \exp\left(-\frac{E_P \cdot N_n - \Delta G^*}{k_B \cdot T}\right) \tag{3}$$

Where N_n is the number of first neighbors, E_D and E_P are the energy barriers for a dissolution and a precipitation event respectively (see Figure 1), and ΔG^* is the local Gibbs free energy.

With this model both dissolution and precipitation are taken into account, and together they describe the net dissolution process. Equation (4) is the classic KMC equation that has been widely used in dissolution kinetics.[25–30] Dissolution is assumed to be intrinsic for a mineral and its topography, via E_D and N_n respectively, and it does not depend on ΔG^*. Equation (5) accounts for precipitation phenomenon, and takes into account the dependence with the solute concentration by means of ΔG^*, and similarly to the dissolution rate equation, the nature of the mineral and topography is considered via E_P and N_n.

Two aspects of the model must be remarked. First, when the system is very far from equilibrium ($\Delta G^* \rightarrow -\infty$) the precipitation rate becomes negligible and the proposed model is then reduced to the usual Arrhenius Equation (1). Second, if the net dissolution rate $r_D - r_P$ is calculated and $E_D = E_P$ and no N_n dependence is considered, the general expression for the normal TST is recovered (Equation (4)).

$$r_D - r_P = A \cdot \left(1 - \exp\left(\frac{\Delta G^*}{k_B \cdot T}\right)\right) \tag{4}$$

where A is a constant.

In Equation (3) the local ΔG^* must be related to the macroscopic ΔG. For that, the kink site is taken as a reference for the mineral dissolution[11,33,34] (see Figure 1a). It is a peculiar position: independently of the mineral composition an atom in this position has always half the number of bonds that in the bulk, and therefore its energy is half. Indeed, it is observed experimentally that the sublimation energy of a crystal corresponds to the change of the internal energy when detaching a kink atom.[11,33,34] With this site as reference, ΔG^* and ΔG for a crystal are related by the following expression if the activity is set to the unity (Equation (5))[33,35]:

$$\Delta G = (\Delta G^* - b) \cdot N_{nK} \tag{5}$$

where N_{nK} is the coordination of a kink site; in a Kossel crystal $N_{nK} = 3$. The constant b can be determined by considering that equilibrium is reached during dissolution when no kink atoms can dissolve $r_D = r_P$, and hence the macroscopic $\Delta G = 0$ (see Equations (6) and (7)):

$$r_D(N_n = N_{nK}) = r_P(N_n = N_{nK}) \rightarrow \Delta G = 0 \tag{6}$$

Expressing the result in $k_B T$ units, the constant b is:

$$b = N_{nK} \cdot (E_P - E_D) \tag{7}$$

2. Experimental Section

The system under study consisted in a Kossel crystal with $240 \times 240 \times 8$ sites for a total of ≈ 460800 with periodic boundary conditions. With a typical distance between atoms of 2.5 Å,[36] the system had a size of $\approx 60 \times 60$ nm. Mineral topography and surface are key factors in the dissolution mechanisms. To simulate a mineral as real as possible all the different topographic defects showed in Figure 1a were included. On the surface, a random number of terraces, vacancies, and adatoms were represented.

The system had two initial dislocations. This equated, for the system size, to a dislocation density of $\approx 5.5 \cdot 10^{10}$ cm^{-2}. This value lies into the known dislocation density range for minerals: $10^6 - 10^{10}$ cm^{-2}.[37] The disposition of the dislocations varies with the crystallographic plane considered. In this paper the simplest case was considered; the {100}, {010} and {001} planes with perpendicular dislocations as they could be appreciated in Figure 1a. An on-lattice KMC home code was developed using C++11 language. Only surface atoms were supposed to react since they were in contact with the solvent; therefore there were no possible events for a bulk atom.

A major problem in simulations close to equilibrium conditions is that sites undergo dissolution and precipitation reactions rapidly. These fast events happen continuously, inducing an exponential increase on the use of computing resources, blocking the simulation. Therefore a methodology to advance in time is necessary, skipping repetitive and computationally time consuming steps. There are several algorithms to avoid such issues,[38–40] yet a new one was used based on Poisson processes statistics, explained in detail in Supporting Information. Briefly, for an atom attempting to dissolve, it is possible to do an estimation of the probability for that atom to truly leave the mineral taking into account both dissolving and precipitation rates. System times are then recalculated based on that probability and plenty of simulation time is saved depending on ΔG value and mineral cohesive energy. While far from equilibrium conditions this does not make any difference, close to it, in a highly cohesive mineral, simulations are about 10^4 times faster.

The next step was to set the values of the model parameters. The activation energy E_a for a dissolution process of a typical mineral lies in the range of $30 \lesssim E_a \lesssim 85$ kJ mol^{-1}.[28] Expressing this in $k_B T$ units ($k_B T = 2.494$ kJ mol^{-1} at 300 K), $12 \lesssim E_a \lesssim 34$. In the model E_D represents the bond breaking energy barrier, which in a Kossel crystal with an average of three broken bonds during a dissolution event, should correspond to $E_a/3$. Hence, simulations with $E_D = 4.0$, 7.0, 9.0, 12.0 $k_B T$ units were done. Several ΔG
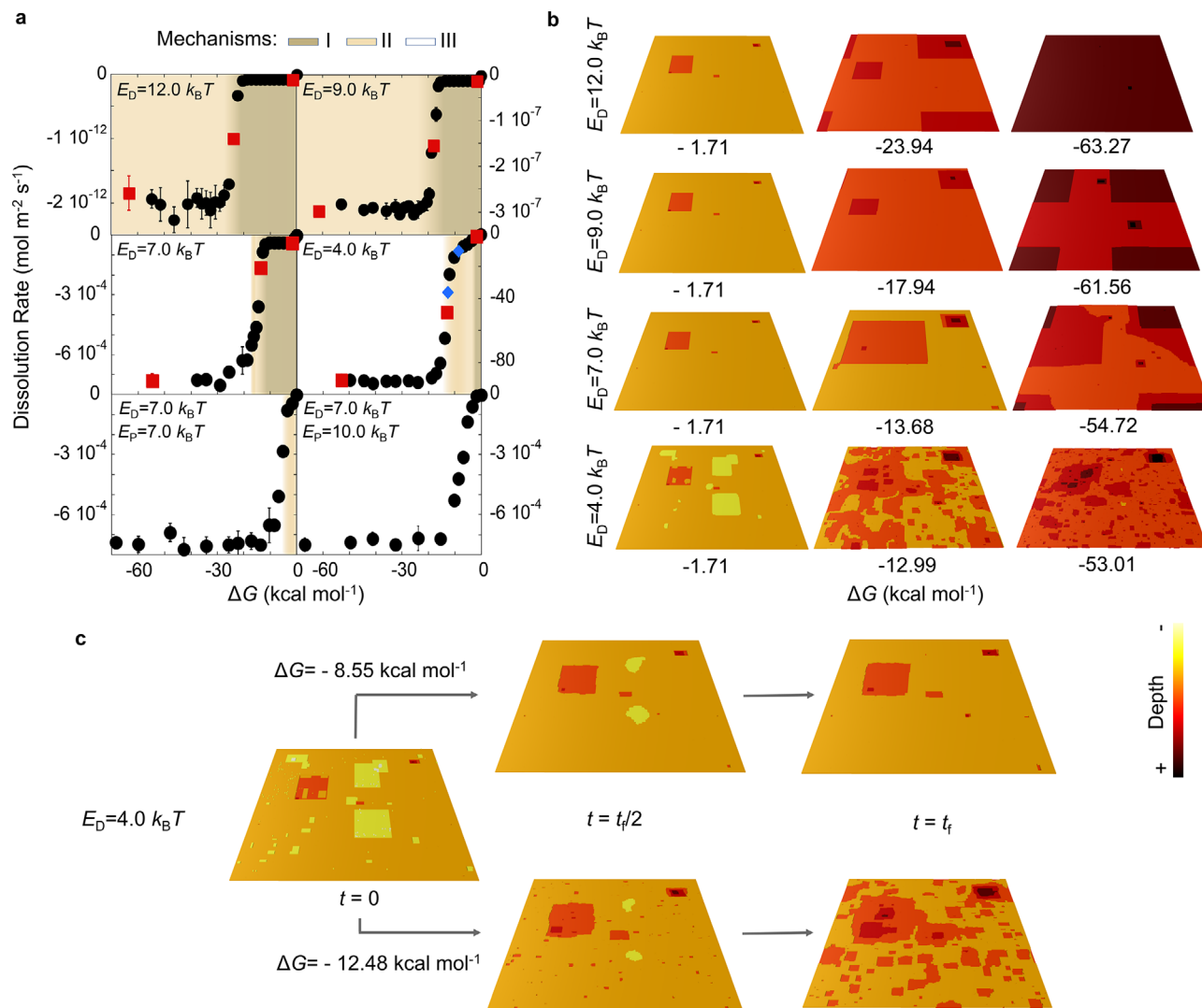
**ADVANCED
SCIENCE NEWS**

www.advancedsciencenews.com

**ADVANCED
THEORY AND
SIMULATIONS**

www.advtheorysimul.com

Figure 2. Dissolution rate versus Gibbs free energy (ΔG). a) Kossel crystal with different precipitation and dissolution energies. Points in red and blue are represented in panels (b) and (c), respectively. b) Surfaces at a given time t_f. c) Time evolution of the surface. The visual representation is done using OVITO program.[42]

values covering the three mechanism zones were taken starting from $\Delta G = 0$ and with finer focus on the ΔG_{crit} onset. For the energy barrier of precipitation events a value of $E_P = 1.0\ k_B T$ units was taken. The fundamental frequency in minerals can range between $\approx 10^{11}$ and $\approx 10^{14}$ s^{-1}.[33,41] A value of $f_f = 4 \cdot 10^{13}$ s^{-1} at $T = 300$ K was considered for this work. Herein, the presented results are the average of 5 simulations for each condition unless the contrary is specified.

3. Results

3.1. Dissolution Rate as a Function of ΔG

First, the effect of E_D on the dissolution rate as a function of ΔG is tested. Simulations with $E_D = 4.0$, 7.0, 9.0, $12.0\ k_B T$ units are shown in **Figure 2**a. It is remarkable that the curves

have the sigmoidal shape found experimentally. To the best of our knowledge this is the first model that reproduces the whole ΔG dependence and captures the inherent mechanism and its topography. Close to $\Delta G = 0$, in mechanism I region, very low dissolution takes place since only adatoms and terraces are dissolved. Then dissolution slowly increases until ΔG is low enough to allow pit opening or mechanism II, leading to a sharp onset. Finally a steady dissolution rate is obtained at very low ΔG values when mechanism III governs dissolution if E_D is low enough. It is important to notice that the relationship between ΔG_{crit} and E_D matches what is seen in experiments; the higher the E_D, the lower the ΔG_{crit}. Another fact of agreement with experiments is the maximum dissolution rate far from equilibrium: the higher the E_D, the lower negative rate.

In Figure 2a the cases $E_D = 7.0\ k_B T$ and $E_P = 7.0\ k_B T$ and $E_P = 10.0\ k_B T$ are studied to show how E_P affects mechanisms and to underline that the TST curve can also be reproduced by the

**ADVANCED
SCIENCE NEWS**
www.advancedsciencenews.com

**ADVANCED
THEORY AND
SIMULATIONS**
www.advtheorysimul.com

model. Two interesting phenomena should be emphasized. On the one hand, mechanisms II and III can take place very close to equilibrium conditions. On the other hand, if E_P is significantly higher than E_D, spontaneous vacancies can be created and pit opening is more favorable than adatom removal, provoking very irregular patterns. To our knowledge, this dissolution mode has not been proposed before and should deserve experimental validation. Though at present we cannot prove it, it seems plausible that this dissolution mode might be involved in the X-ray driven dissolution instabilities observed by Laanait et al. [43] in Calcite-water interfaces.

In Figure 2b dissolution patterns are represented in the three differentiated zones for the four cases in Figure 2a. First, at high cohesive energies, $E_D = 12.0\ k_B T$ and $E_D = 9.0\ k_B T$, two dissolution mechanisms are easily differentiated. Close to equilibrium only terraces and adatoms are dissolved (mechanism I). Once ΔG_{crit} is reached, dissolution is produced almost exclusively from step retreat (mechanism II). Mechanism III does not exist in these cases. Second, looking at minerals with low cohesive energies $E_D = 7.0\ k_B T$ and $E_D = 4.0\ k_B T$, it can be seen that, like in the previous case, at close to equilibrium conditions adatoms and terraces are the only ones which are removed. Once ΔG_{crit} is reached pits start to open. But shortly after ΔG_{crit} value, spontaneous opening of surface (mechanism III) happens, the more the farther from equilibrium. At far from equilibrium conditions differences in energy between more and less coordinated atoms are not high enough to prevent them to dissolve closed to randomness, so very irregular patterns are produced.

The difference between mechanisms becomes more evident the lower the E_D is. Therefore, for a better sighting, in Figure 2c the dissolution pattern at three different times in the onset between mechanism II and mechanism III for a $E_D = 4.0\ k_B T$ mineral is shown. In minerals with low cohesive energy, in addition to the contribution to dissolution rate of the dislocation opening, there is certain contribution from mechanism III.

3.2. Calculation of ΔG_{crit} as a Function of E_D and E_P

Dislocations are key structural features for the mineral dissolution. It is validated in this work that in all studied cases dislocations produce the onset in the dissolution rate at ΔG_{crit}.[9,27,44,45] Once the system is able to remove an atom close to dislocations, that is, with four neighbors in a Kossel crystal, the dissolution probability of the atoms in that layer increases due to the appearance of three-coordinated kink site atoms. It is possible to analytically relate the microscopic variables E_D and E_P used in this model with the macroscopic ΔG_{crit} by Equation (8) demonstrated in Supporting Information:

$$\Delta G_{crit}(k_B T \text{ units}) \approx \left(\alpha - b - N_{nD} \cdot (E_D - E_P)\right) \cdot N_{nK} \tag{8}$$

where N_{nD} is the coordination number for an atom close to a dislocation (see Figure 1a,d), $N_{nD} = 4$ for a Kossel crystal. α value is determined in the supplementary information to report ΔG_{crit} at its middle height value: $\alpha = -2.3 \pm 0.9\ k_B T$. The accuracy of Equation (8) is checked in **Table 1**. There is an excellent match between the ΔG_{crit} value obtained from simulations and the one calculated analytically when the transition between mechanism I

Table 1. Validation of Equation (8). ΔG_{crit} is obtained by applying the Equation (10), which is later explained, to Figure 2b. E_D and E_P are in $k_B T$ units. Error in analytical ΔG_{crit} is ± 1.6 kcal mol^{-1} (see Figure S2, Supporting Information).

E_D	E_P	Simulation ΔG_{crit} [kcal mol^{-1}]	Analytical ΔG_{crit} [kcal mol^{-1}]
12.0	1.0	−24	−23.8
9.0	1.0	−18	−18.4
7.0	1.0	−15	−14.9
7.0	7.0	−2	−4.1
7.0	10.0	−7	1.3
4.0	1.0	−13	−9.5

and II takes place at a negative ΔG. It must be noted that according to expression 8, for a given mineral with a fix E_D, ΔG_{crit} also depends on E_P. Therefore different dissolution mechanisms and rates can be experimentally reported even with the same mineral and ΔG. It is also interesting to point that the analytical expression allows to determine the theoretical ΔG_{crit} even in conditions where E_P is higher than E_D and the onset is produced at positive ΔG. Indeed, this behavior has been observed by Juilland and Galluci in alite.[10]

3.3. Relationship between E_D and E_a

TST proposes dissolution as a set of elementary reactions that can take place if the system is able to overcome an energy barrier determined by an Arrhenius equation.[11]

$$R = A' \cdot \exp\left(-\frac{E_a}{k_B \cdot T}\right) \tag{9}$$

Where A' is a constant.

The activation energy in the Arrhenius equation is in fact an apparent energy because it compiles the contribution from many terms and not just the energy barrier of the elementary reactions. In this sense, the supplementary information includes a deeper study concerning the fundamental frequency dependence with temperature, which is closely related to the dissolution rate (see Equation (1)).

In the idealized simulation model the activation energy E_a can be written as $E_a = N_{nK} \cdot E_D$ because it is observed experimentally that the sublimation energy of a crystal corresponds to the change of internal energy when detaching a kink atom. Nevertheless, as it is checked below, this relation is not true at the whole ΔG range.[22] In the next step, the real link between macroscopic E_a and microscopic E_D is explored to compare with the experimental data.

Experimental studies usually report a single E_a, usually corresponding to far from equilibrium conditions in a grain shape system. Nevertheless, in an infinite surface system E_a actually depends on the dissolution mechanism. In the mechanism I zone, dissolution is driven by removal of kink atoms in terraces. In contrast, in mechanisms II/III zones dissolution is driven by step retreat. Therefore, microscopically, it is expected that $E_{a\ m.I} \approx$
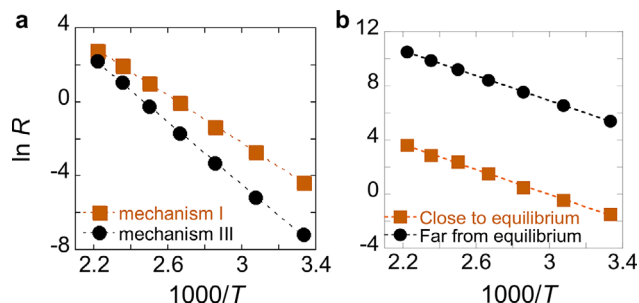
ADVANCED
SCIENCE NEWS
www.advancedsciencenews.com

ADVANCED
THEORY AND
SIMULATIONS
www.advtheorysimul.com

Figure 3. Natural logarithm of dissolution rate ln R versus $1000/T$. a) Kossel crystal of $E_D = 7.0\ k_B T$ and $E_P = 1.0\ k_B T$ units. b) Same values for a diamond-like mineral. Points in black represent far from equilibrium conditions. Points in orange represent close to equilibrium conditions. Error is smaller than the size of the points. Arrhenius fitting parameters are represented in Table 2.

Table 2. Activation energy and fitting parameters. Reported values in Figure 3 for both, a Kossel crystal in mechanisms III and I, and a four coordinated diamond like mineral at far from equilibrium (f.f.e) and close to equilibrium conditions (c.e). The latter is studied in the supplementary information.

		Kossel crystal	Diamond-like system
Mech. III / f.f.e	ln A'	20.98 ± 0.19	20.69 ± 0.05
	$\frac{E_a}{E_D}$	4.0	2.2
	E_a	70.5 ± 0.6 kJ mol^{-1}	38.0 ± 0.2 kJ mol^{-1}
Mech. I / c.e	ln A'	17.15 ± 0.06	13.8 ± 0.3
	$\frac{E_a}{E_D}$	3.1	2.2
	E_a	53.73 ± 0.17 kJ mol^{-1}	38.3 ± 0.9 kJ mol^{-1}

$N_{nK} \cdot E_D$ and $E_{a\,m.II/III} \approx N_{nD} \cdot E_D$, where N_{nK} and N_{nD} are 3 and 4 respectively for a Kossel crystal (see **Figure 3**a and **Table 2**).

In order to verify such relationship, Arrhenius equation has been used to fit the natural logarithm of the dissolution rate ln R as a function of the inverse of T for fixed ΔG conditions corresponding to mechanisms I and III. For that, values of 7 $k_B T$ and 1 $k_B T$ units have been chosen for E_D and E_P respectively. For the mechanism III, the Kossel crystal described before has been used, and the dissolution rate at each T is taken as the plateau value at far from equilibrium conditions. However, to study mechanism I, a limiting value of the reaction rate R is not reached. For this case, the beginning of the ΔG_{crit} onset represents a good reference point since no contributions from other mechanisms are involved. In addition, the Kossel crystal topography has been modify for a better quantification of the rate. As only terraces dissolution is the governing mechanism, a surface with a big terrace of eight sites high has been constructed without any other surface defect.

As it can be seen in Figure 3a, there is good linear correlation of dissolution rate logarithm with the inverse of temperature for both mechanisms, which indicates that the systems are following an Arrhenius process as expected. An important consequence is that the expected values of E_a as a function of E_D are obtained ($E_{a\,m.I} = 3.1 \cdot E_D$ and $E_{a\,m.II/III} = 4.0 \cdot E_D$). Therefore, the macroscopic dissolution activation energy can be obtained directly from the computed dissolution reaction energy in any ΔG conditions.

3.4. Comparison with Experimental Dissolution Rates

Next target is to apply the proposed model to describe the experimentally reported dissolution for several minerals: albite,[12,27] smectite,[13,27] alite,[17] labradorite,[18,27] and K-feldspar.[46] **Table 3** contains the obtained values for the model parameters in Equations (2) and (3), their activation energies, and the ΔG_{crit}.

The initial values for the simulations have been set as follows. First the ΔG_{crit} value is obtained from the empirical Equation (10). Note that both this empirical equation and Equation (8) report ΔG_{crit} at the middle height value. Second, a guess E_D value is chosen based on the dissolution rate limit value at far from equilibrium conditions. Finally, E_P is calculated from Equation (8). With these initial values simulations are run and the parameters are adjusted ad hoc to obtain the best possible fit according to the regression coefficient between the simulation results and an empirical fit for the experimental data.

The experimental and computed dissolution rates as a function of ΔG are shown in **Figure 4**. Besides, an empirical fitting function that differs from the previously proposed in the state of the art[12,34] is shown. The fitting function adds a logistic function term[47] to the TST expression, and reads as in Equation (10):

$$R = A \cdot \left(1 - \exp\left(\frac{\Delta G}{k_B \cdot T}\right)\right)$$
$$+ B \cdot \left(1 - \frac{1}{1 + \exp(D \cdot (-\Delta G + \Delta G_{crit}))}\right) \quad (10)$$

where A and B are the limiting dissolution rates corresponding to close and far from equilibrium conditions respectively, and D is a fitting parameter related to E_D and topography.

From Figure 4 it can be first noticed that the sigmoidal shape of the mineral dissolution rate as a function of ΔG can be reproduced with the presented model. Furthermore, Equation (8) provides a ΔG_{crit} in good agreement with the experimental and computed values and helps to define the onset in cases in which transition between mechanism I and II is not so clear, such as the case of K-feldspar.

The dissolution and precipitation energies E_D and E_P, the activation energies in mechanism I and II regions, and the ΔG_{crit} obtained from the fitting are presented in Table 3, together with experimental dissolution activation energies. All the obtained values are in reasonable orders of magnitude, yet the experimental dissolution activation energies are consistently overestimated by nearly a factor of 2 for all minerals. Clearly, using a Kossel crystal with the same topography for all the studied minerals will necessary lead to qualitative results. In addition, there is a dependency of the dissolution rate with the dislocation density.[37,48–51] Such dependency has been tested with the presented model and reveals that the dislocation density is in particular important for high E_D minerals at far from equilibrium conditions (see Supporting Information). Other discrepancies in the values can arise from considering a ΔG value independent of ion activities, the unknown initial surface conditions, or the homogeneous fundamental frequency value chosen for the study.

**ADVANCED
SCIENCE NEWS**
www.advancedsciencenews.com

**ADVANCED
THEORY AND
SIMULATIONS**
www.advtheorysimul.com

Table 3. Model parameters for minerals. Fitting values for Figure 4 of the corresponding activation energy in each mechanism and comparison with bibliographic ones. ΔG_{crit} value obtained by Equation (10) and analytically by Equation (8). (*) This value is obtained experimentally in a plane with dislocation opening.

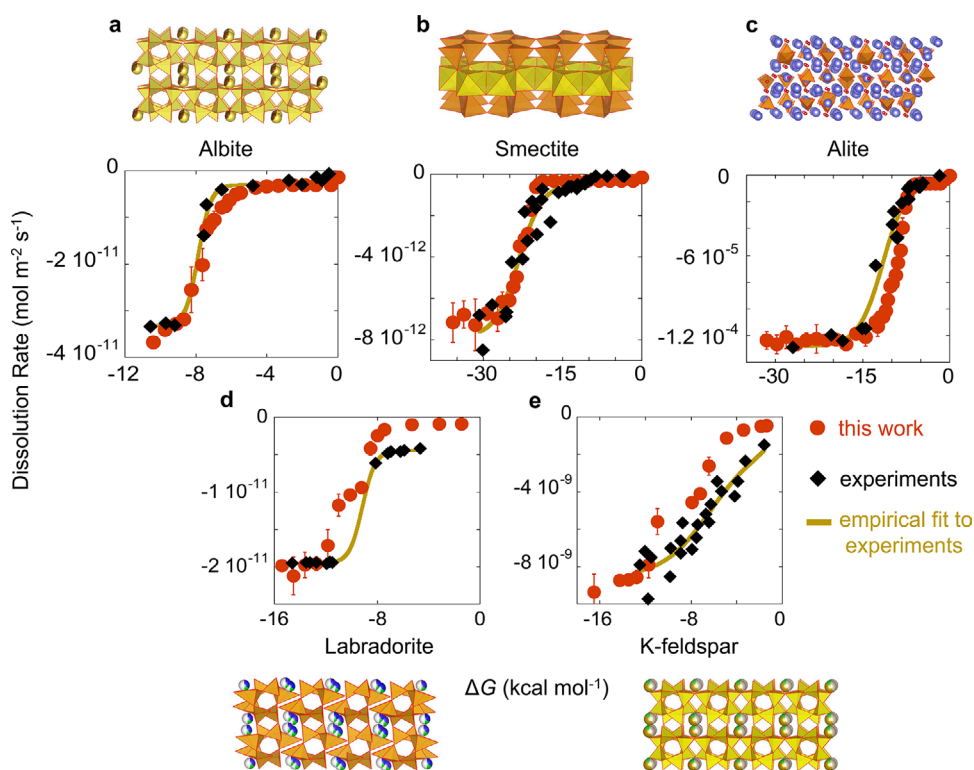| Mineral	T (K)	$E_D (k_B T)$	$E_P (k_B T)$	$E_{a\ m.II/III}$ (kJ mol^{-1})	$E_{a\ m.I}$ (kJ mol^{-1})	$E_{a\ exp.}$ (kJ mol^{-1})	Simulation ΔG_{crit} (kcal mol^{-1})	Analytical ΔG_{crit} (kcal mol^{-1})
Albite	357	11.14	10.00	132	99	69.8 [53]	−8	−7.3 ± 1.9
						71 ± 7 [54]		
						88.6 [55]		
						69 ± 5 [56]		
Smectite	357	11.73	4.00	139	104	52 ± 4 [57]	−23	−21.4 ± 1.9
Alite	300	7.47	4.95	75	56	49* [10]	−11	−8.6 ± 1.6
Labradorite	300	11.40	8.8	114	85	45.2 [53]	−9	−8.8 ± 1.6
Feldspar	423	9.95	10.3	139	104	38.0 [53]	−6	−5 ± 2

Figure 4. Comparison of the experimental data with the proposed dissolution theory. a) Albite at pH 8.8 and 357 K.[12,27] b) Smectite at pH 3 and 357 K.[13,27] c) Alite at 300 K.[17] d) Labradorite at pH 3 and 300 K.[18,27] e) K-feldspar at pH 9 and 423 K.[46] Structural visualization is done using VESTA program.[52]

4. Conclusions

In this work a new atomistic mineral dissolution model is presented. Based on a KMC protocol, the main novelty of the model consists in taking into account the microscopic reversibility of chemical reaction by adding a new precipitation term to the usual TST dissolution equation. As a result, it is possible for the first time to reproduce the experimentally observed sigmoidal dependence of the dissolution rate over the whole ΔG range by atomistic simulations. Indeed, as proof of concept, the two main parameters of the model (the dissolution and precipitation energies) have been calibrated to correctly fit the dissolution rates of several representative minerals. Besides, and what is most important, the model successfully captures the proposed dissolution mechanisms and their activation. The three observed dissolution mechanisms naturally emerge from the simulations depending on dissolving energy E_D and ΔG: initial irregularities dissolution (mechanism I) at close to equilibrium conditions, pit opening and step retreat (mechanism II) when ΔG_{crit} is reached, and spontaneous vacancy opening (mechanism III) at far from

equilibrium conditions when the E_D is low enough. The model also confirms the generally accepted idea that the onset for the dissolution rate increase is originated by the opening of pits, which constantly supplies terraces for step retreat. Interestingly, according to the simulations, when the dissolution and precipitation energies are sufficiently low and high respectively, there can exist close-to-equilibrium dissolution modes where spontaneous vacancies creation and pit opening can occur before adatom and terrace removal. These dissolution modes have not been previously reported, and should deserve due experimental attention.

In summary, the present model sheds new light on the subtle dissolution mechanisms, and can open the door to the development of a comprehensive theoretical framework for dissolution and other surface-related phenomena like etching [58]. Future works will be focused on building realistic mineral models beyond the current implementation based on simple Kossel crystals.

Supporting Information

Supporting Information is available from the Wiley Online Library or from the author.

Conflict of Interest

The authors declare no conflict of interest.

[1] N. Van Breemen, P. Buurman, *Soil Formation*, Springer Science & Business Media, New York **2002**.
[2] K. Kalbitz, S. Solinger, J.-H. Park, B. Michalzik, E. Matzner, *Soil Sci.* **2000**, *165*, 277.
[3] H. R. Krouse, C. A. Viau, L. S. Eliuk, A. Ueda, S. Halas, *Nature* **1988**, *333*, 415.
[4] M. Canals, J. D. Meunier, *Geochim. Cosmochim. Acta* **1995**, *59*, 699.
[5] R. Lal, *Philos. Trans. R. Soc., B* **2008**, *363*, 815.
[6] R. Lal, *Science* **2004**, *304*, 1623.
[7] S. Blain, B. Quéguiner, L. Armand, S. Belviso, B. Bombled, L. Bopp, A. Bowie, C. Brunet, C. Brussaard, F. Carlotti, U. Christaki, A. Corbiere, I. Durand, F. Ebersbach, J. L. Fuda, N. Garcia, L. Gerringa, B. Griffiths, C. Guigue, C. Guillerm, S. Jacquet, C. Jeandel, P. Laan, D. Lefevre, C. Lo Monaco, A. Malits, J. Mosseri, I. Obernosterer, Y. H. Park, M. Picheral, et al., *Nature* **2007**, *446*, 1070.
[8] D. E. Giammar, R. G. Bruant Jr, C. A. Peters, *Chem. Geol.* **2005**, *217*, 257.
[9] P. Juilland, E. Gallucci, R. Flatt, K. Scrivener, *Cem. Concr. Res.* **2010**, *40*, 831.
[10] P. Juilland, E. Gallucci, *Cem. Concr. Res.* **2015**, *76*, 180.
[11] A. C. Lasaga, *Kinetic Theory in the Earth Sciences*, Princeton University Press, Princeton, NJ **2014**.
[12] T. Burch, K. Nagy, A. Lasaga, *Chem. Geol.* **1993**, *105*, 137.
[13] J. Cama, J. Ganor, C. Ayora, C. A. Lasaga, *Geochim. Cosmochim. Acta* **2000**, *64*, 2701.
[14] J. Xu, C. Fan, H. H. Teng, *Chem. Geol.* **2012**, *322*, 11.
[15] R. S. Arvidson, A. Luttge, *Chem. Geol.* **2010**, *269*, 79.
[16] L. Nicoleau, M. A. Bertolim, *J. Am. Ceram. Soc.* **2016**, *99*, 773.
[17] L. Nicoleau, A. Nonat, D. Perrey, *Cem. Concr. Res.* **2013**, *47*, 14.
[18] A. S. Taylor, J. D. Blum, A. C. Lasaga, *Geochim. Cosmochim. Acta* **2000**, *64*, 2389.
[19] A. Lüttge, *J. Electron Spectrosc. Relat. Phenom.* **2006**, *150*, 248.
[20] C. Fischer, I. Kurganskaya, A. Luttge, *Appl. Geochem.* **2018**, *91*, 140.
[21] A. C. Lasaga, A. E. Blum, *Geochim. Cosmochim. Acta* **1986**, *50*, 2363.
[22] A. C. Lasaga, A. Lüttge, *Am. Mineral.* **2004**, *89*, 527.
[23] A. F. Voter, in *Radiation Effects in Solids*, Springer, New York **2007**, pp. 1–23.
[24] Y. Liang, D. R. Baer, J. M. McCoy, J. E. Amonette, J. P. Lafemina, *Geochim. Cosmochim. Acta* **1996**, *60*, 4883.
[25] I. Kurganskaya, A. Luttge, *J. Phys. Chem. C* **2013**, *117*, 24894.
[26] I. Kurganskaya, A. Luttge, *J. Phys. Chem. C* **2016**, *120*, 6482.
[27] A. C. Lasaga, A. Luttge, *Science* **2001**, *291*, 2400.
[28] P. Meakin, K. M. Rosso, *J. Chem. Phys.* **2008**, *129*, 204106.
[29] L. Briese, R. S. Arvidson, A. Luttge, *Geochim. Cosmochim. Acta* **2017**, *212*, 167.
[30] C. Fischer, A. Luttge, *Proc. Natl. Acad. Sci.* **2018**, *115*, 897.
[31] L. Zhang, A. Lüttge, *Am. Mineral.* **2007**, *92*, 1316.
[32] L. Zhang, A. Lüttge, *Geochim. Cosmochim. Acta* **2009**, *73*, 2832.
[33] K. Oura, M. Katayama, A. Saranin, V. Lifshits, A. Zotov, *Surface Science*, Vol. *602*, Springer, Berlin **2003**.
[34] S. L. Brantley, J. D. Kubicki, A. F. White, *Kinetics of Water–Rock Interaction*, Vol. 168, Springer, Berlin **2008**.
[35] J. Z. Bandstra, S. L. Brantley, *Geochim. Cosmochim. Acta* **2008**, *72*, 2587.
[36] G. V. Gibbs, R. T. Downs, D. F. Cox, N. L. Ross, C. T. Prewitt, K. M. Rosso, T. Lippmann, A. Kirfel, *Z. Kristallogr. Cryst. Mater.* **2008**, *223*, 01.
[37] H. Teng, *Geochim. Cosmochim. Acta* **2004**, *68*, 253.
[38] A. Chatterjee, A. F. Voter, *J. Chem. Phys.* **2010**, *132*, 194101.
[39] E. C. Dybeck, C. P. Plaisance, M. Neurock, *J. Chem. Theory Comput.* **2017**, *13*, 1525.
[40] M. Jørgensen, H. Grönbeck, *J. Chem. Phys.* **2018**, *149*, 114101.
[41] A. Putnis, *An Introduction to Mineral Sciences*, Cambridge University Press, Cambridge **1992**.
[42] A. Stukowski, *Modell. Simul. Mater. Sci. Eng.* **2010**, *18*, 015012.
[43] N. Laanait, E. B. Callagon, Z. Zhang, N. C. Sturchio, S. S. Lee, P. Fenter, *Science* **2015**, *349*, 1330.
[44] P. M. Dove, N. Han, J. J. De Yoreo, *Proc. Natl. Acad. Sci.* **2005**, *102*, 15357.
[45] C. Fischer, R. S. Arvidson, A. Lüttge, *Geochim. Cosmochim. Acta* **2012**, *98*, 177.

**ADVANCED
SCIENCE NEWS**

www.advancedsciencenews.com

**ADVANCED
THEORY AND
SIMULATIONS**

www.advtheorysimul.com

[46] J.-M. Gautier, E. H. Oelkers, J. Schott, *Geochim. Cosmochim. Acta* **1994**, *58*, 4549.

[47] D. G. Zill, *A First Course in Differential Equations with Modeling Applications*, Cengage Learning, Boston, MA **2012**.

[48] G. Holdren, W. Casey, H. Westrich, M. Carr, M. Boslough, *Chem. Geol.* **1988**, *70*, 79.

[49] W. H. Casey, M. J. Carr, R. A. Graham, *Geochim. Cosmochim. Acta* **1988**, *52*, 1545.

[50] J. Schott, S. Brantley, D. Crerar, C. Guy, M. Borcsik, C. Willaime, *Geochim. Cosmochim. Acta* **1989**, *53*, 373.

[51] R. T. Cygan, W. H. Casey, M. B. Boslough, H. R. Westrich, M. J. Carr, G. R. Holdren Jr, *Chem. Geol.* **1989**, *78*, 229.

[52] K. Momma, F. Izumi, *J. Appl. Crystallogr.* **2008**, *41*, 653.

[53] J. L. Palandri, Y. K. Kharaka, *A Compilation of Rate Parameters of Water-Mineral Interaction Kinetics for Application to Geochemical Modeling*, U.S. Geological Survey, Menlo Park, CA **2004**.

[54] N. Rose, *Geochim. Cosmochim. Acta* **1991**, *55*, 3273.

[55] H. C. Helgeson, W. M. Murphy, P. Aagaard, *Geochim. Cosmochim. Acta* **1984**, *48*, 2405.

[56] Y. Chen, S. L. Brantley, *Chem. Geol.* **1997**, *135*, 275.

[57] A. Bauer, G. Berger, *Appl. Geochem.* **1998**, *13*, 905.

[58] X. Ye, M. R. Jones, L. B. Frechette, Q. Chen, A. S. Powers, P. Ercius, G. Dunn, G. M. Rotskoff, S. C. Nguyen, V. P. Adiga, A. Zettl, E. Rabani, P. L. Geissler, A. P. Alivisatos, *Science* **2016**, *354*, 874.